Journal of Petroleum Exploration and Production Technology
https://doi.org/10.1007/s13202-024-01805-8

ORIGINAL PAPER-EXPLORATION ENGINEERING

Automatic arrival-time picking of P- and S-waves of micro-seismic events based on relative standard generative adversarial network and GHRA

Jianxian Cai[1] · Zhijun Duan[1] · Fenfen Yan[1] · Yuzi Zhang[1] · Ruwang Mu[1] · Huanyu Cai[1] · Zhefan Ding[1]

Received: 26 October 2023 / Accepted: 1 April 2024

Abstract

Rapid, high-precision pickup of microseismic P- and S-waves is an important basis for microseismic monitoring and early warning. However, it is difficult to provide fast and highly accurate pickup of micro-seismic P- and S-waves arrival-time. To address this, the study proposes a lightweight and high-precision micro-seismic P- and S-waves arrival times picking model, lightweight adversarial U-shaped network (LAU-Net), based on the framework of the generative adversarial network, and successfully deployed in low-power devices. The pickup network constructs a lightweight feature extraction layer (GHRA) that focuses on extracting pertinent feature information, reducing model complexity and computation, and speeding up pickup. We propose a new adversarial learning strategy called application-aware loss function. By introducing the distribution difference between the predicted results and the artificial labels during the training process, we improve the training stability and further improve the pickup accuracy while ensuring the pickup speed. Finally, 8986 and 473 sets of micro-seismic events are used as training and testing sets to train and test the LAU-Net model, and compared with the STA/LTA algorithm, CNNDET+CGANet algorithm, and UNet++ algorithm, the speed of each pickup is faster than that of the other algorithms by 11.59ms, 15.19ms, and 7.79ms, respectively. The accuracy of the P-wave pickup is improved by 0.221, 0.01, and 0.029, respectively, and the S-wave pickup accuracy is improved by 0.233, 0.135, and 0.102, respectively. It is further applied in the actual project of the Shengli oilfield in Sichuan. The LAU-Net model can meet the needs of practical micro-seismic monitoring and early warning and provides a new way of thinking for accurate and fast on-time picking of micro-seismic P- and S-waves.

Keywords Arrival-time picking of P- and S-waves · Generative adversarial network · Lightweight feature extraction (GHRA) · Application-aware loss function

List of symbols

AvgPool	Average pooling operation
$a = G(z)$	The result of arrival-time picking of the LAU-Net model.
D	The discriminator network
$f^{7\times1}$	The convolution kernel is a 71 one-dimensional convolution operation
$f_{(\tilde{1})}$, $f_{(\tilde{2})}$, and $f_{(\tilde{3})}$	functions that need to be determined

Z. Duan, F. Yan, Y. Zhang and R. Mu have contributed equally to this work.

✉ Zhijun Duan
dzj_0108@163.com

Jianxian Cai
cjxlaq@163.com

Fenfen Yan
337856275@qq.com

Yuzi Zhang
1401803365@qq.com

Ruwang Mu
864838684@qq.com

Huanyu Cai
3030583022@qq.com

Zhefan Ding
466438789@qq.com

[1] Hebei Key Laboratory of Seismic Disaster Instrument and Monitoring Technology, Langfang 065201, China

Published online: 11 May 2024

FP	The count of instances where a non-P- and S-wave is incorrectly picked as a micro-seismic P- and S-wave arrival time
FN	The count of times a micro-seismic P- and S-wave arrival time is missed
G	The pickup network
$G(z)$	Picked sample
MaxPool	Maxpooling operation
MLP	Multilayer perception operation
$p(\tilde{z})$	Specific distribution
TP	The count of correctly picked micro-seismic P- and S-wave's arrival times
v_i	The amplitude value of the micro-seismic waveform
x	The amplitude value of the MS waveform
x_i	The output of the one-dimensional Ghost convolutional layer
x_i'	The output of the channel attention mechanism
x_i''	The output of the spatial attention mechanism.
$\tilde{x}_r^D$	The artificial labeling of the input discriminant network
$\tilde{x}_f^G$	The new pickup result
$\tilde{x}_f^D$	The pickup network picking up the P- and S-waves result of the input discriminant network
y	The new pickup result
z	Training wave
$\times$	Training wave
σ	The sigmoid function
$\oplus$	Concat operation
$\otimes$	A fusion operation of different channels
λ	Hyperparameters in Eq. (5)

Abbreviations

AIC	Akaike information criterion
CF	Characteristic function
CNN	Convolutional neural network
DL	Deep learning
FD	Fractal dimension
GAN	Generative adversarial network
GRU	Gated recurrent unit
GHRA	A lightweight feature extraction layer
HRA	Hybrid attention mechanism
IM	Inactivity method
LR	Learning rate
LSGAN	Least squares generative adversarial network
LSTM	Long-short-term memory
MAE	Mean absolute error
MB	MByte
MSSA	Multi-channel singular spectrum analysis
P	Precision
R	Recall
RSGAN	Relative standard generative adversarial network
SNR	Signal-to-noise ratio
STA/LTA	Short-time and long-time averaging ratio
VFD	Variance fractal dimension

Introduction

The micro-seismic monitoring system integrates micro-seismic sensors and data recording equipment, which can be used to record the full waveform data of micro-vibrations from underground rocks and strata (Fahd et al. 2023; Dandi et al. 2023; Xu et al. 2021). By picking up the P- and S-waves of the micro-seismic events, the location of the micro-seismic source can be obtained, and a fast and accurate early warning of micro-seismic can be realized (Alireza and Mojdeh 2023). The study of how to quickly and accurately pick up the P- and S-waves of micro-seismic events has become a key core for seismic signal processing.

At present, there are two main categories of micro-seismic P- and S-waves arrival-time pickup methods: traditional methods and deep learning (DL) methods. Traditional methods mainly include the short-term and long-term average ratio (STA/LTA) (Deyu et al. 2023), the Akaike information criterion (AIC) (Lan et al. 2022), and the fractal dimension (FD) (Tiwari and Rajesh 2021). These ideas were developed by Xu and Chen (2021) proposed a new characteristic function (CF) based on the modified cumulative envelope function to improve the ability of the STA/LTA method to identify P- and S- waves. Yao and Liu (2022) proposed an automatic seismic P-wave first-arrival pickup algorithm based on the inactivity method (IM) and the Akaike information criterion (AIC), which minimizes the noise interference and can pick up the first arrival time even when using a data set with a low signal-to-noise ratio (SNR). Avoiding noise interference, P-waves can be picked up even when using datasets with low SNR. Long et al. (2023) proposed an automatic micro-seismic event detection variance fractal dimension (VFD) method based on multi-trace energy envelope stacking (MTEES), which improves the micro-seismic event detection accuracy for micro-seismic monitoring. These methods rely heavily on manually designed features and rules, which not only limit their ability to extract P- and S-wave features from micro-seismic events, resulting in low

P- and S-wave pickup accuracy, but also are not suitable for fast processing of a large number of signals acquired by a large number of micro-seismic monitoring systems.

In recent years, deep learning techniques have made greater progress and have been widely applied in various fields, especially providing new solutions to the problem of fast and accurate pickup of P- and S-waves (Fahd et al. 2021; ERTURUL 2019). Compared with traditional P- and S-wave pickup methods, deep learning-based pickup methods have obvious advantages in terms of accuracy, speed, and robustness (Alakbari et al. 2023; Acar et al. 2021). This approach has found widespread application in the realm of pickup of P- and S-waves as Guo et al. (2021) designed the AEnet model, which uses a convolutional neural network (CNN) to classify the sample points, and combines the curve-fitting technique and unsupervised clustering algorithm to calculate the sample point arrivals to prevent incorrectly labeling the noise as P- and S- waves, but the micro-seismic waveforms have a short duration, and the effect of picking up the P- and S- waves are poor in the low-resolution waveforms. Xu et al. (2022) pioneered the use of the multi-channel singular spectrum analysis (MSSA) method to mitigate the effect of noise on micro-seismic waveforms, and then utilized a long short-term memory network (LSTM) for accurate temporal feature extraction, but the method was unable to extract detailed features, and the accuracy of the pickups was reduced when compared to convolutional neural networks. Guo (2021) introduced the UNet++ model with a wide receptive field to capture complex waveform details and enhance the distinction between P- and S-waves and noise. The model can determine the micro-seismic P- and S- wave arrival time directly from waveforms interfered with by background noise. However, the micro-seismic signals are time-series data, and the effect of the time-series information on the waveform feature extraction is not considered. Jiao et al. (2023) used a deep convolutional model for micro-seismic event detection. Subsequently, they utilized the timing processing capability of the gated recursive unit (GRU) and the detail processing function of the self-attention mechanism to accurately determine the P- and S-waves arrival time. The result was a substantial improvement in accuracy to 0.98, but the model complexity was high.

The development of micro-seismic P- and S-wave pickup algorithms faces the following challenges: (1) Micro-seismic signal acquisition is significantly affected by complex environments, such as periodic industrial interference noise and impulse noise from mechanical or human vibration in the field. These noises make it difficult for the model to fully extract the P- and S-wave features, resulting in low P- and S-wave pickup accuracy. (2) Since micro-seismic monitoring systems need to operate for long periods, low-power devices are often used to be able to ensure that the system maintains stable operation with limited energy supply, reduce maintenance costs, and extend the service life of the system. However, current algorithms increase the number of parameters and computational complexity of the model to be able to improve the accuracy of picking up P- and S-waves from complex environments, to the point where they are not adapted to low-power devices and the pickup speed slows down. Addressing these challenges is critical to achieving fast and accurate pickup results. However, the reduction of model parameters can make P- and S-wave feature extraction inadequate, which leads to low accuracy. Therefore, it is critical for P- and S-wave pickup models to balance both accuracy and speed for optimal performance.

Motivated by the above analysis, this study addresses the low accuracy and slow speed of the current micro-seismic P- and S-wave pickup methods. In this study, we propose a new P- and S-wave method called LAU-Net. The LAU-Net model draws on the idea of generative adversarial and consists of a pickup network and a discriminative network. The pickup network employs Ghost convolution and hybrid attention mechanism (HRA) to acquire semantic and detailed information for P efficiently- and S-waves while maintaining a lightweight structure to improve the pickup speed; the discriminative network focuses on capturing valuable details and avoiding picking up noise as P- and S-waves to improve the pickup accuracy of the model.

In summary, our advantages are summarized as follows:

1. The LAU-Net model uses a pickup-discriminative network structure. The pickup network focuses on improving the pickup speed; the discriminative network focuses on improving the pickup accuracy.
2. Replacing the ordinary convolutional layer of the U-shaped network with a lightweight feature extraction layer and using it as a pickup network reduces the model parameters and speeds up the model pickup speed. The lightweight feature extraction layer consists of Ghost convolution and hybrid attention mechanism (HRA), which utilizes its advantage of selectively enhancing P- and S-wave features with fewer parameters to achieve better pickup of P- and S-waves.
3. The LAU-Net model is designed with an application-aware loss function to achieve higher model pickup accuracy. This function helps the pickup network to understand the pickup errors and improves its pickup accuracy by eliminating the errors of P- and S-wave arrivals with manual labeling.

The rest of this study is organized as follows: Section 2 provides an insight into the proposed LAU-Net model, discussing its overall structure and main modules. Section 3 focuses on the dataset and evaluation metrics. Section 4 presents the analysis of the experimental results. Finally, Section 5 concludes the paper.

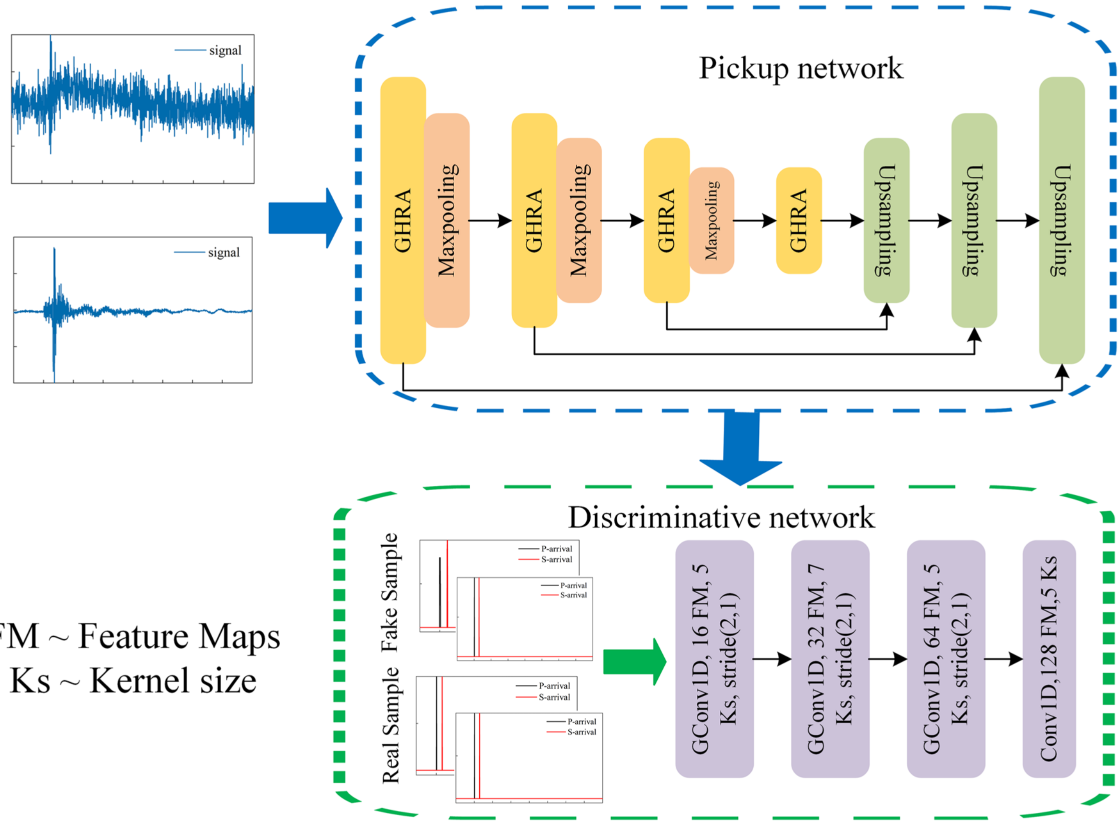

Fig. 1 LAU-Net model structure

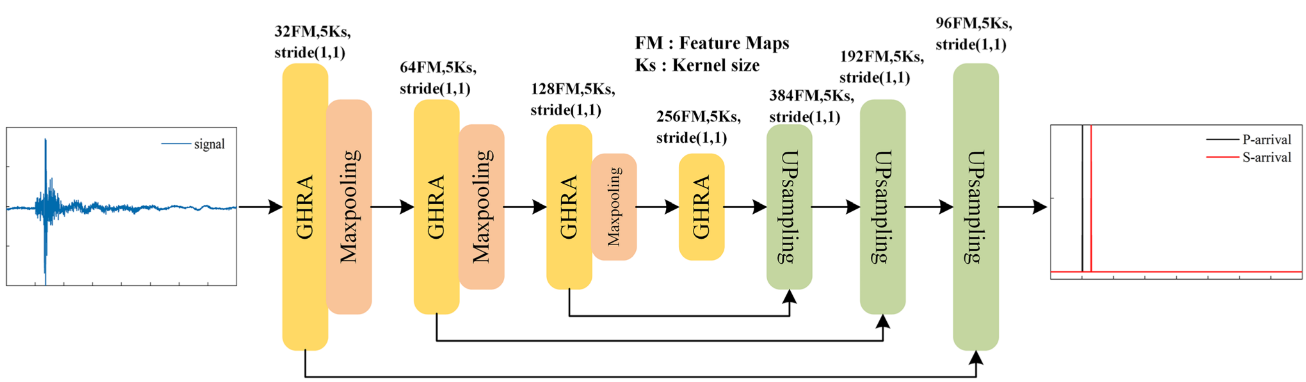

Fig. 2 GHRA layer structure

Method

LAU-Net model structure

The study employs a generative adversarial network (GAN) (Goodfellow et al. 2020) as its framework, and the architecture of the LAU-Net model is illustrated in Fig. 1. The LAU-Net model comprises two key components: the pickup network and the discriminative network.

The pickup network, represented by the blue dashed box, integrates the lightweight feature extraction layer (GHRA), the maxpooling layer, and the upsampling layer to facilitate the task of micro-seismic P- and S-waves picking. The green dashed box represents the discriminative network, which incorporates a one-dimensional Ghost convolutional layer. This layer plays a crucial role in further constraining the direction of gradient updates for the pickup network.

Table 1 Details of pickup network

Name	Details	Size
Input		1600
GHRA layer	GhostConv1×5 Str.1	1600
Maxpooling layer	Maxpooling1×2	800
GHRA layer	GhostConv1×5 Str.1	800
Maxpooling layer	Maxpooling1×2	400
GHRA layer	GhostConv1×5 Str.1	400
Maxpooling layer	Maxpooling×2	200
GHRA layer	GhostConv1×5 Str.1	200
Upsampling layer	Conv.Trans1×5 Str.2;GhostConv1×5 Str.1	400
Upsampling layer	Conv.Trans1×5 Str.2;GhostConv1×5 Str.1	800
Upsampling layer	Conv.Trans1×5 Str.2;GhostConv1×5 Str.1	1600
Output	Conv1×1 Str.1	1600

Pickup networks

The pickup network is mainly composed of four GHRA layers, three maxpooling layers, and three upsampling layers, and the structure is shown in Fig. 2. The 1D micro-seismic signals are first extracted from the GHRA and maxpooling layers. Then, the upsampling layers are used to achieve accurate P- and S-wave arrival-time pickup. Table 1 lists the details of the pickup network.

To reduce the model's parameters, the paper substitutes the convolution operation within the U-Net structure with a lightweight feature extraction layer known as GHRA (lightweight feature extraction). The GHRA layer's structure is illustrated in Fig. 3. The GHRA layer is an amalgamation of the 1D Ghost convolutional layer (Han et al. 2022) and the hybrid residual attention (HRA) module (Li et al. 2022). This combination serves to diminish the number of parameters and extract prominent features by using the HRA module, all while consolidating the salient information via the 1D Ghost convolutional layer. This approach results in a feature layer enriched with substantial information. Firstly, the paper employs a 1D Ghost convolutional layer to filter the input data and generate a feature map. The output of the 1D Ghost convolution layer serves as the input for the HRA module. The HRA module initially employs the channel attention mechanism [e.g., Eq. (1)] to establish correlations among similar micro-seismic waveforms across different channels, emphasizing micro-seismic P- and S-wave arrival times in a clean channel. Subsequently, it utilizes the spatial attention mechanism [e.g., Eq (2)] to enhance the micro-seismic P- and S-waves arrival-times features by correlating any two samples in the micro-seismic P- and S-waves waveforms with each other. The two calculations are shown in Eqs. (1–2) (Tang et al. 2021):

$$x_i' = (\sigma(MLP(AvgPool(x_i)) + MLP(MaxPool(x_i)))) \otimes x_i \quad (1)$$

$$x_i'' = (\sigma(f^{7\times1}(AvgPool(x_i);MaxPool(x_i))) \otimes x_i' \quad (2)$$

where σ is the sigmoid function, x_i is the output of the one-dimensional Ghost convolutional layer, x_i' is the output of the channel attention mechanism, and x_i'' is the output of the spatial attention mechanism.$\otimes$ denotes the fusion operation of different channels, MaxPool denotes the maximum pooling operation, AvgPool denotes the average pooling operation, MLP denotes the multilayer perception operation, and $f^{7\times1}$ denotes the one-dimensional convolution operation with a $f^{7\times1}$ convolution kernel.

A maxpooling layer consists of a maximum pooling layer. After the feature map is max-pooled, its length and width will be reduced to half of the original.

An upsampling layer consists of a transpose convolution layer and a GHRA layer. The upsampling layer first expands the length and width of the feature map to twice the original one by a transposition convolution operation. Secondly, the GHRA layer is used to achieve feature fusion of different channels.

Discriminative network

The excessive non-P- and S-wave samples within micro-seismic waveforms significantly disrupt the process of picking P- and S-wave arrival times. In response to this challenge, the study introduces a fully convolutional discriminative network to replace the discriminator that was originally designed for overall classification in the adversarial network. In contrast to other methods, the LAU-Net model produces a confidence curve as its output rather than a scalar value. Each sample point within the output confidence curve indicates whether the corresponding input sample point represents a picked result or a genuine label. The absence of a fully connected layer in the fully convolutional network allows it to process input waveforms of varying sizes, further enhancing the versatility of the LAU-Net model for P- and S-wave arrival-time pickup tasks. The structure of the discriminative network is illustrated in Fig. 1. The inputs to this network are categorized as "real samples" and "fake samples." "Real samples" represent artificial labels, while "fake samples" arise from the combination of artificial labels and model-picking outputs in the depth dimension. The discriminative network utilizes three one-dimensional Ghost convolutional layers and one conventional convolutional layer. These layers consist of feature maps with dimensions of 16, 32, 64, and 128, accompanied by convolutional kernel sizes of 5, 7, 5, and 5, respectively.

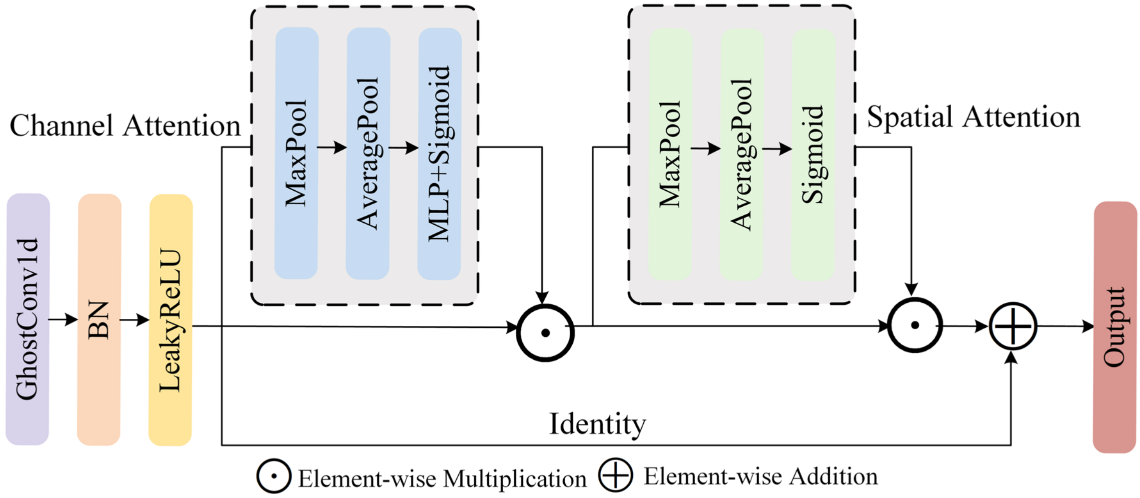

Fig. 3 Structure of the pickup network

Application-aware loss function

When the parameters of the pickup network are fewer, the network may be less effective for the segmentation of fine cracks in the image, partly because of the insufficient feature extraction ability of the network with fewer parameters, and partly because the traditional error function of the statistics of sampling points one by one can not effectively respond to the distance between the artificial samples and the pickup results. The adversarial generative network defines a distance that can be trained, and it is hoped that this distance is as big as possible when training a discriminative network, and it is hoped that this distance is as small as possible when training a generative network. Therefore, the idea of relative standard generative adversarial network (RSGAN) (Jolicoeur-Martineau 2018) can be borrowed to measure the distance between the prediction result and the artificial label by a trainable discriminative network. If the discriminative network is unable to discriminate the results of the pickup network picking up P- and S-waves, it can be assumed that the pickup network has been trained well enough. Similarly, the pickup network needs the help of manually labeled P- and S-wave results for optimal training so that it can be constantly compared and improved. The loss function of RSGAN is shown in Eq. (3) (Jolicoeur-Martineau 2018).

$$\begin{aligned} L_D &= E_{x_r\sim p(x),x_f=G(z),z\sim p(\tilde{z})}\left[\tilde{f}_1(D(\tilde{x_r^D}))\right] \\ &\quad E_{x_r\sim p(x),x_f=G(z),z\sim p(\tilde{z})}\left[\tilde{f}_2(D(\tilde{x_f^D}))\right] \\ L_G &= E_{x_r\sim p(x),x_f=G(z),z\sim p(\tilde{z})}\left[\tilde{f}_3(D(\tilde{x_f^G}))\right] \end{aligned} \tag{3}$$

D denotes the discriminative network and G denotes the pickup network. x_r represents the manual labeling result which obeys the distribution $p\,(x)$. x_f represents the pickup network picking up the P- and S-waves result, which obeys the distribution $p(\tilde{z})$. $\tilde{x_r^D}$ denotes the artificial labeling of the input discriminant network, i.e., $\tilde{x_r^D} = x_r \oplus x_r$, $\tilde{x_f^D}$ denotes the pickup network picking up the P- and S-waves result of the input discriminant network, i.e., $\tilde{x_f^D} = x_f \oplus x_r$. $\tilde{x_f^G}$ denotes the new pickup result, i.e., $\tilde{x_r^G} = x_r \oplus x_f$. $\oplus$ denotes the splicing operation of the manual labels and the model pickup results at the input. $f_(\tilde{1})$, $f_(\tilde{2})$, and $f_(\tilde{3})$ denote the inputs as a function of the outputs.

The design of the three functions $f_(\tilde{1})$, $f_(\tilde{2})$, and $f_(\tilde{3})$ draws on the least squares adversarial network (LSGAN) (Mao et al. 2017), where the least squares function is used to force the pickup results of the pickup network to approximate the artificial labels to improve the accuracy of the P- and S-wave pickup. Therefore, Eq. (3) can be further rewritten as Eq. (4) (Mao et al. 2017):

$$\begin{aligned} L_D &= E_{x_r\sim p(x),x_f=G(z),z\sim p(\tilde{z})}\left[D(\tilde{x_r^D}) - 1\right] \\ &\quad + E_{x_r\sim p(x),x_f=G(z),z\sim p(\tilde{z})}\left[D(\tilde{x_f^D}))\right] \\ L_G &= E_{x_r\sim p(x),x_f=G(z),z\sim p(\tilde{z})}\left[D(\tilde{x_f^G}) - 1\right] \end{aligned} \tag{4}$$

For the parameter update of the pickup network, in addition to the error of the discriminative network, the error between the artificial labels and the pickup network should be taken into account. The final application-aware loss function of the LAU-Net model can be expressed as (Ni et al. 2022):

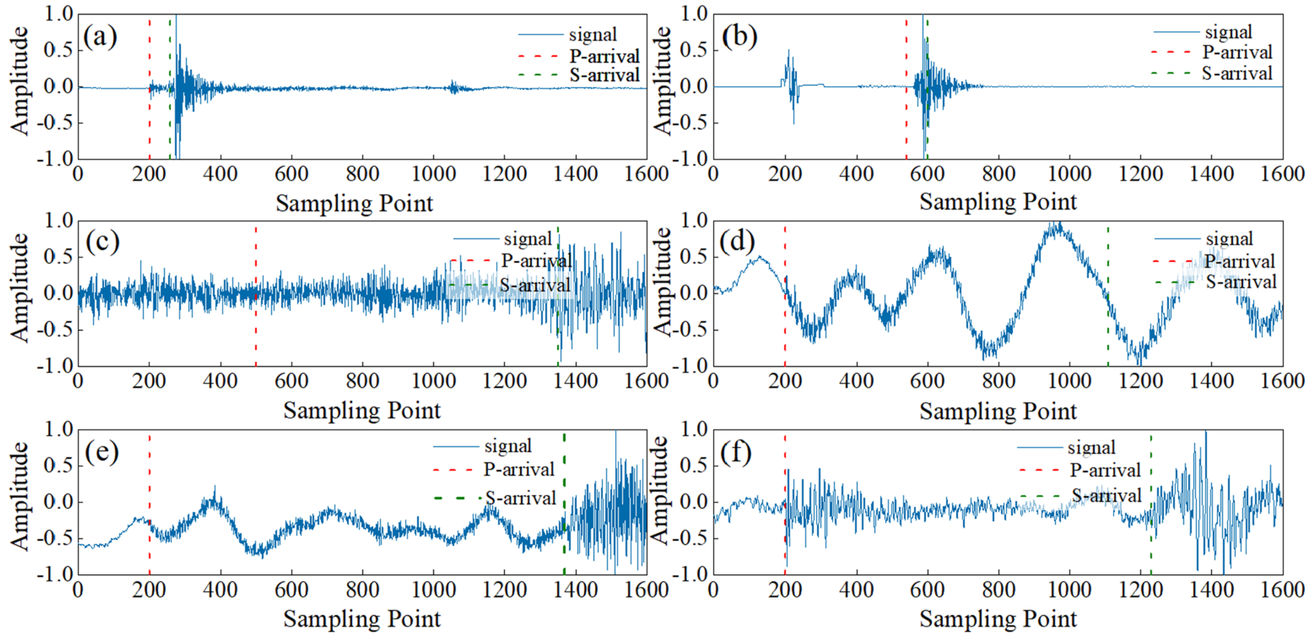

Fig. 4 Micro-seismic waveform data and their labels

$$
\begin{aligned}
L_D &= E_{x_r \sim p(x), x_f = G(z), z \sim p(\tilde{z})}[D(\tilde{x_r^D}) - 1] \\
&\quad + E_{x_r \sim p(x), x_f = G(z), z \sim p(\tilde{z})}[D(\tilde{x_f^D}))] \\
L_G &= -\frac{1}{n}\sum\nolimits_x [ylna - (1-y)ln(1-a)] \\
&\quad + \lambda \times E_{x_r \sim p(x), x_f = G(z), z \sim p(\tilde{z})}[D(\tilde{x_f^G}) - 1]
\end{aligned}
\tag{5}
$$

where y denotes the result of manual labeling and $a = G(z)$ denotes the result of arrival-time pickup of the LAU-Net model.

Data pre-processing and evaluation indicators

Datasets

The dataset utilized in this study comprises data collected from the ground-based micro-seismic monitoring system at Shengli Oilfield, Sichuan, during the years 2011–2017. Micro-seismic waveforms were recorded using a network of nine broadband three-component micro-seismic stations deployed across the oilfield. These stations covered a spatial range of approximately 6 km × 4 km × 1 km and originally sampled data at a frequency of 5 kHz. In this study, to obtain more comprehensive and accurate subsurface information for the study of subsurface structures or monitoring of subsurface activities, clean micro-seismic waveforms, waveforms with low SNRs, and micro-seismic waveforms with indistinguishable arrival-time of P- and S-wave, totaling 9,459 micro-seismic waveforms, were selected. Among them, the selection of P- and S-wave arrival time was carefully carried out by micro-seismic experts. The results of multiple experts were considered together, and then these results were converted into corresponding confidence probability labels to form a high-quality dataset. Some of the data in the dataset are shown in Fig. 4.

The study employs 473 data samples for the test set, while the remaining 8986 data samples are allocated to the training and testing sets. All pertinent methods have been trained and tested, a necessity for supervised deep learning models, and subsequently evaluated using the same dataset to ensure a fair and unbiased comparison of their strengths and weaknesses. The data have been uniformly normalized, as depicted in Eq. (6) (Cai et al. 2022), where v_i denotes the amplitude value of the micro-seismic waveform.

$$
v_i = \frac{v_i}{max|v_i|} \tag{6}
$$

Evaluation indicators

To quantitatively showcase the effectiveness of the LAU-Net model, three metrics—precision (P), recall (R), and F1-score—were employed to assess the quantitative model's performance. The mathematical computations for precision, recall, and F1-score are presented in Eqs. (9), (10), and (11) (Hou and Zheng 2023):

$$P = \frac{\mathrm{TP}}{\mathrm{TP} + \mathrm{FP}} \tag{7}$$

$$R = \frac{\mathrm{TP}}{\mathrm{TP} + \mathrm{FN}} \tag{8}$$

$$F1 - \text{score} = 2 \times \left(\frac{P \times R}{P + R} \right) \tag{9}$$

where TP denotes the count of correctly picked micro-seismic P/S-wave arrival times, FP signifies the count of instances where a non-P- and S-wave is incorrectly picked as a micro-seismic P- and S-wave arrival time, and FN represents the count of times a micro-seismic P- and S-wave arrival time is missed. A higher recall leads to a reduction in the number of missed picks of micro-seismic P- and S-wave arrival times, while higher precision results in fewer instances of missed micro-seismic P- and S-wave arrival times. Due to the trade-off between recall and precision, the F1 score provides a balanced and weighted combination of the two.

Experiments

The experimental setup in this paper involved using the Python 3.8 interpreter and the PyTorch 1.0 deep learning framework to construct the model. Experimental tests were conducted on an RTX 3060 GPU with an AMD Ryzen R7-5800 H processor. The paper underwent multiple iterations to fine-tune the parameters within both the discriminative and picking networks. In each iteration, the discriminative network's parameters were updated using waveform inputs, followed by fixing these parameters and updating the parameters within the picking network using another set of waveform inputs. This process was repeated for each iteration. A total of 4493 waveforms were used to train the discriminative network during each cycle, with another 4493 waveforms used to train the pickup network.

In this section, we validate the accuracy and speed of the LAU-Net model for picking up P- and S-waves through different experiments. To assess the effect of model convolution kernel size on pickup speed and accuracy (as described in Sect. 4.1), we select five different convolution kernel sizes and compare their performances on the Sichuan micro-seismic dataset from 2011–2017 to select the optimal convolution kernel size. To evaluate the effect of model depth on pickup speed and accuracy (as described in Sect. 4.2), we designed three model configurations and compared their performance on the 2011–2017 Sichuan micro-seismic dataset to select the optimal number of layers. To demonstrate the stability of the LAU-Net model, we evaluate it on the 2011–2017 Sichuan micro-seismic dataset in Sect. 4.3. To demonstrate the effectiveness of introducing blocks in the LAU-Net model, we compare and evaluate the 2011–2017 Sichuan micro-seismic dataset in Sect. 4.4. Subsequently, in Sect. 4.5, we fully analyze and compare the performance of the LAU-Net model with existing methods. Furthermore, in Sect. 4.6, we apply the LAU-Net model to the 2019–2020 Sichuan micro-seismic dataset, thus highlighting its practical applicability and generalization capability. In Sect. 4.7, we consider the adaptability of the LAU-Net model to pickup P- and S-waves under different signal-to-noise ratios and different kinds of noise. Finally, in Sect. 4.8 we discuss the limitations of the LAU-Net model and suggest directions for future work.

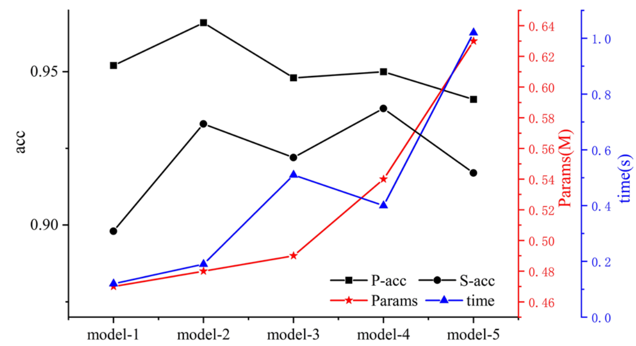

Fig. 5 Test results of models 1–5

Convolutional kernel size selection

To assess the influence of various convolutional kernel sizes on the determination of P- and S-waves arrival times, the paper formulates five models based on the LAU-Net approach outlined in "Section 2.2." Models 1 through 5 utilize convolutional kernel sizes of 3, 5, 11, 31, and 71, respectively. The test results are depicted in Fig. 5. Among these models, model-2 achieves the highest precision in P-wave arrival-time determination, model-4 excels in S-wave arrival-time precision, and model-1 possesses the most minimal parameter count. This illustrates that smaller convolution kernels result in incomplete extraction of S-wave features, leading to diminished precision in S-wave arrival-time determination. Conversely, larger convolution kernels enhance S-wave arrival-time precision but may capture redundant information from the micro-seismic waveforms, resulting in decreased precision in P-wave arrival-time determination. Thus, while varying the convolution kernel size can refine model precision and increase parameter counts, selecting the most precise yet lightweight structure among the five models remains a challenging task.

Table 2 P-wave and S-wave arrival-times pickup effects of the three different models

Model	P-wave				S-wave				Params/MB	Time (ms)
	P	R	F1	MAE (s)	P	R	F1	MAE (s)		
LAU-Net-3GHRA	0.978	0.971	0.974	0.316	0.858	0.950	0.902	1.706	0.19	1.41
LAU-Net-4GHRA	0.983	0.986	0.984	0.129	0.966	0.969	0.967	0.159	0.48	3.11
LAU-Net-5GHRA	0.981	0.979	0.980	0.161	0.957	0.959	0.958	0.234	2.27	7.41

For instance, if prioritizing model size, model-1 emerges as the optimal choice. On the other hand, if focusing solely on accuracy, model-2 delivers the highest precision in P-wave arrival-time determination, and model-4 excels in S-wave arrival-time determination precision. The S-wave arrival-time determination precision of model-2 is comparable to that of model-4, and model-4 has 1.125 times the parameters of model-1.

To meet the requirement of achieving high precision while maintaining relatively modest model complexity for micro-seismic P- and S-wave arrival-time pickup, the study selects model-2 as the neural network structure for the P- and S-wave arrival-time pickup task.

Optimization of the number of model layers

The layer count in the LAU-Net model significantly impacts the speed and precision of P- and S-wave arrival-time determination. To identify the optimal depth for the number of layers in the LAU-Net model, three distinct model architectures are devised. These structures involve 3, 4, and 5 GHRA layers, respectively denoted as LAU-Net-3GHRA, LAU-Net-4GHRA, and LAU-Net-5GHRA. A comparative assessment of precision, recall, F1-score, mean absolute error (MAE), model parameter sizes, and runtime is presented in Table 2.

Table 2 furnishes valuable insights into the performance of various LAU-Net model configurations. LAU-Net-4GHRA exhibits noteworthy improvements in precision for both P-wave and S-wave arrival-time determination, with gains of 0.05 and 0.108 in the former, and 0.015 and 0.019 in the latter for recall. It also reduces the mean absolute error (MAE) by 0.187 for P-waves and 1.547 for S-waves compared to LAU-Net-3GHRA. Furthermore, the MAE for P-wave arrival-time determination between LAU-Net-5GHRA and LAU-Net-4GHRA is nearly identical, suggesting that these two networks provide more consistent P-wave arrival-time determination performance compared to LAU-Net-3GHRA. However, concerning S-wave arrival-time determination, LAU-Net-4GHRA enhances precision by 0.009, recall by 0.01, and reduces the MAE by 0.075 compared to LAU-Net-5GHRA. In terms of model complexity, LAU-Net-4GHRA features 1.79MB fewer model parameters and operates 1.7ms faster than LAU-Net-5GHRA, while having 0.29MB more model parameters and running 4.3ms slower than LAU-Net-3GHRA.

To achieve an equilibrium between elevated precision in the pickup and a judiciously controlled model complexity for the determination of micro-seismic P- and S-wave arrival times, the paper opts for LAU-Net-4GHRA as the architectural framework for the pickup network.

Cross-validation experiments

To accurately assess the generalization performance of the LAU-Net model, fivefold cross-validation was used. The entire dataset was equally divided into 5 subsets, each of which was rotated as a test set, while the remaining 4 subsets were used as a training set for model training. In the training set, the data was randomly divided into 80% for training and 20% for validation. The training data is used to build the best classification model, while the validation data is used to refine the network structure. Throughout 50 epochs, the model is trained on the training data and evaluated on the validation data for each epoch. The model with the highest classification accuracy on the validation data was retained and subsequently tested on the test set. At the end of each phase, the precision, recall, F1 score, and mean absolute error of the models picking up the P- and S-waves were calculated, and the final results were determined by averaging the fivefold cross-validation results. Table 3 shows the fivefold cross-validation results, with P-wave precision ranging from 0.949 to 0.983, recall ranging from 0.87 to 0.986, F1 scores ranging from 0.92 to 0.984, and mean absolute errors ranging from 0.029s to 0.135s, and S-wave precision ranging from 0.888 to 0.966 and recall ranging from 0.85 to 0.947, with the F1 scores between 0.869 and 0.956 with mean absolute errors between 0.039s and 0.194s.

Ablation experiments

Ablation experiments were conducted to assess the influence of the GHRA layer and the application-aware loss function in the LAU-Net model on the overall model performance. These experiments compared three model variations: the U-shaped micro-seismic P- and S-wave arrival-time pickup model (Ablation model U-Net), a variation that substitutes the convolutional layer with the GHRA layer

Table 3 Cross-validation experiment results

Model	P-wave				S-wave				Params/MB	Time (ms)
	P	R	F1	MAE (s)	P	R	F1	MAE (s)		
1k-fold	0.958	0.941	0.949	0.116	0.888	0.850	0.869	0.176	0.48	3.11
2k-fold	0.983	0.986	0.984	0.029	0.966	0.947	0.956	0.039	0.48	3.11
3k-fold	0.971	0.969	0.97	0.061	0.937	0.929	0.933	0.194	0.48	3.11
4k-fold	0.949	0.939	0.944	0.104	0.946	0.937	0.941	0.065	0.48	3.11
5k-fold	0.969	0.87	0.92	0.135	0.928	0.892	0.91	0.086	0.48	3.11
Mean	0.966	0.941	0.953	0.059	0.934	0.922	0.928	0.104	0.48	3.11

Table 4 Results of the ablation experiments

Model	P-wave				S-wave				Params/MB	Time (ms)
	P	R	F1	MAE	P	R	F1	MAE		
U-Net	0.884	0.856	0.870	0.169s	0.842	0.807	0.824	0.259s	0.82	7.41
LU-Net	0.858	0.826	0.842	0.184s	0.816	0.754	0.784	0.286s	0.46	2.61
LAU-Net	0.966	0.941	0.953	0.089s	0.933	0.911	0.922	0.11s	0.48	3.11

(Ablation model LU-Net), and the LAU-Net model introduced in the paper. All experiments utilized the complete dataset for both training and testing. The results are presented in Table 4. Table 4 reveals the experiment outcomes. In contrast to the LAU-Net model proposed in the paper, the ablation model U-Net exhibits reduced precision in picking both P-waves and S-waves by 0.082 and 0.091, respectively. It also increases model parameters by 0.34MB and slows down processing speed by 4.3ms. The ablation model LU-Net shows a similar decline in precision, with reductions of 0.108 for P-waves and 0.117 for S-waves. However, it manages to decrease model parameters by 0.02MB and accelerates processing by 0.5ms. Notably, the ablation model U-Net has the most model parameters, while the ablation model LU-Net has the fewest. This underscores the effectiveness of the designed GHRA layer in reducing model complexity and parameters. However, the reduction of model parameters results in decreased model precision. The incorporation of the application-aware loss function, as outlined in the paper, serves to enhance model precision while ensuring the reduction of model parameters.

The hyperparameters in the LAU-Net model have a great impact on the pickup effect, for this reason, the paper selects several sets of parameters for training through several validations of the training set and compares the results. The learning rate, batch size, and loss function hyperparameter size λ and period of the LAU-Net model are adjusted and selected. In each experiment, all parameters except the test parameters are kept constant.

The learning rate (LR) is a key hyperparameter in the field of deep learning and plays a pivotal role in determining whether and when a model can effectively converge to a minimum. This study explores several common learning rates, specifically LR = 0.000001, LR = 0.000005, LR = 0.00001, LR = 0.00005, LR = 0.0001, and LR = 0.0005, and the results in Fig. 6a show that the accuracy rate reaches its optimal value when LR = 0.0001. This is because too high a learning rate will cause the network to fail to converge and the model accuracy will decrease; too low a learning rate will prolong the convergence time of the network and reduce the model training speed. Therefore, 0.0001 is chosen as the learning rate for LAU-Net model training in this study.

Batch size plays a crucial role in optimizing the model and determining the training speed. To speed up the training process of gradient descent algorithms, batch size is usually used to the power of 2. In this study, the batch size of the LAU-Net model was evaluated for 16, 32, 64, 128, and 256 and the results are shown in Fig. 6b. The model accuracy reaches its maximum when its value is 64, and after reaching the maximum, the accuracy starts to decrease as the batch size increases. This is because too small a batch size will make the training time longer and less efficient, while too large a batch size will lead to a decrease in the generalization ability of the model. Therefore, the study chooses 64 as the batch size.

To develop effective P- and S-wave pickup models, the training process requires the selection of appropriate epochs. One epoch represents one training iteration, including forward and backward propagation for all batches. In this study, the LAU-Net model was evaluated for 40, 50, and 60 epochs and the results are shown in Fig. 6c. The value of accuracy is maximum when epoch = 50. This is because at epoch = 40, the model does not learn enough micro-seismic P- and S-wave features, which leads to a lower accuracy rate and makes the model pickup ineffective; at epoch = 60, the

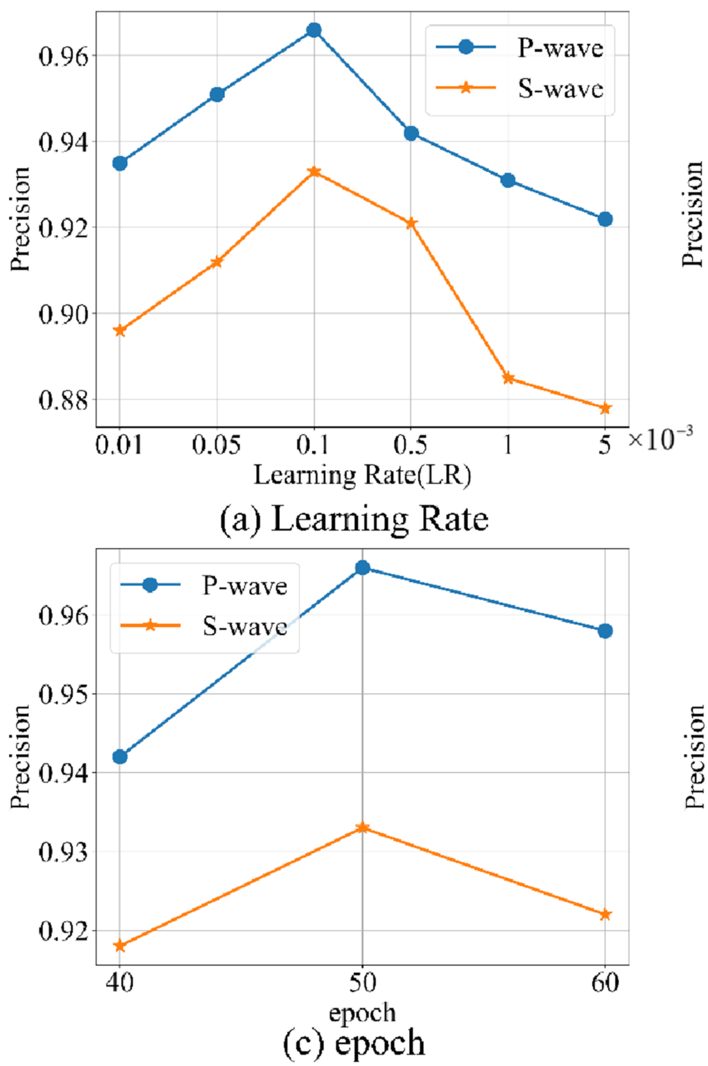

Fig. 6 Effect of different parameters on pickup accuracy

model training falls into the overfitting phenomenon, which leads to a model denoising effect that is not as good as at epoch=50. Therefore, this paper chooses epoch=50 as the epoch of LAU-Net model training.

λ is an important parameter in Eq. (5), which also affects the testing accuracy. In this section, sizes of 0.005, 0.01, 0.05, and 0.1 are chosen to test the LAU-Net model. The test results are shown in Fig. 6d, and from Fig. 6d, it can be seen that the highest accuracy is 96.6% and 93.3% when the size of λ is 0.005, which is higher than the other parameters, so we choose the size of 0.005.

The LAU-Net model was trained 50 times on the training dataset using the ADAM optimizer (Kingma and Ba 2014). The batch size was set to 64 with a learning rate of 0.0001 and was 0.0001 in Eq. (5).

Comparative experiments

To showcase the exceptional prowess of the LAU-Net model, it was employed to analyze data from the microseismic events recorded in the Shengli Oilfield, Sichuan, during 2020. In this investigation, three distinct methods for P- and S-wave arrival-time determination were chosen for comparison. These methods included a conventional short-term average/long-term average (STA/LTA) picker (Allen 1978) and two deep learning-based architectures, namely CAGNET+CNNDET (Jiao et al. 2023) and U-Net++ (Guo 2021). These were evaluated against the LAU-Net model introduced in this study. The traditional P- and S-wave arrival-time determination method employed the Obspy package (Beyreuther et al. 2010), while the deep

Table 5 P-wave and S-wave arrival-times pickup effects of the four different methods on the test set

Model	P-wave				S-wave				Params (MB)	Time (ms)
	P	R	F1	MAE (s)	P	R	F1	MAE (s)		
LAU-Net	0.966	0.941	0.953	0.059	0.934	0.922	0.928	0.104	0.48	1.11
STA/LTA	0.745	0.712	0.728	0.239	0.701	0.698	0.699	0.328	\	12.7
CNNDET+CGANET	0.965	0.94	0.952	0.130	0.799	0.752	0.775	0.291	2.88	16.3
UNet++	0.937	0.923	0.93	0.09	0.88	0.832	0.855	0.180	1.50	8.9

learning-based methods utilized PyTorch for implementation and were trained on a dataset comprising 8986 training samples. All methods were assessed using 473 test samples. As the micro-seismic monitoring datasets varied in time frames, containing micro-seismic waveforms of different lengths, preprocessing was applied to the micro-seismic data following the methodology outlined in Section 3.1.2 of the study. Adjustments were made to the input size and feature clipping layers of the CAGNET+CNNDET and U-Net++ methods to ensure compatibility with the dataset used in this study.

Table 5 exhibits the outcomes of P- and S-wave arrival-time determination for the micro-seismic dataset obtained from the Shengli Oilfield in Sichuan. The results presented in Table 5 showcase that the LAU-Net model attains the highest precision for the determination of both P- and S-wave arrival times, coupled with remarkable recall and F1 scores. Specifically, LAU-Net outperforms the STA/LTA method, demonstrating a precision improvement of 0.221 for P-waves and 0.233 for S-waves. Additionally, it exhibits an increased recall of 0.229 for P-waves and 0.135 for S-waves, as well as F1-score improvements of 0.177 for P-waves and 0.298 for S-waves. Furthermore, the LAU-Net model reduces the mean absolute error (MAE) by 0.175s for P-waves and 0.207s for S-waves. In comparison to the CNNDET+CGANET method, the LAU-Net model achieves a precision increase of 0.001 for P-waves and 0.135 for S-waves. Additionally, it raises recall by 0.001 for P-waves and 0.17 for S-waves, enhancing F1-scores by 0.001 for P-waves and 0.153 for S-waves. Moreover, it decreases the MAEs by 0.071s for P-waves and 0.187s for S-waves. Compared to the UNet++ method, LAU-Net enhances precision by 0.029 for P-waves and 0.054 for S-waves, accompanied by increased recall of 0.018 for P-waves and 0.09 for S-waves. Additionally, it improves F1-scores by 0.023 for P-waves and 0.073 for S-waves, while reducing the MAE by 0.031s for P-waves and 0.076s for S-waves.

The experimental results in Table 5 highlight the superiority of the LAU-Net model as it possesses the highest accuracy, recall, and lowest absolute error. It demonstrates the ability to pickup P- and S-waves in the micro-seismic engineering of the Shengli oilfield in Sichuan and also highlights the superiority of the LAU-Net model in picking up micro-seismic P- and S-waves with accuracy and speed. This is because the STA/LTA method manually designs the amplitude and frequency features, which requires a lot of domain knowledge and experience, and requires repeated attempts for each micro-seismic signal before the corresponding features and thresholds can be found, and thus is slower and less accurate when a large amount of micro-seismic data is processed. The CNNDET+CGANET method needs to go through two networks, with more model parameters and is slow in picking up speed. In addition, the GRU unit and the self-attention mechanism module used in the CNNDET+CGANET method have a long dependency problem for long series time data, which leads to a significant decrease in the accuracy of S-wave when processing waveforms with long time data. The deep structure of the UNet++ method requires a large amount of memory with more model parameters, which leads to low pickup accuracy in resource-constrained environments and slow speed in real-time applications. In real-time applications, the speed is slow. In contrast, the GHRA layer of the LAU-Net model improves the sensitivity to subtle waveform variations by sharing part of the convolution kernel computation, considering the correlation of multiple features in the micro-seismic signals, reducing the model parameters, and accelerating the model to pickup P- and S-waves. In addition, the application-aware loss function in the LAU-Net model can learn complex micro-seismic waveform features, which improves the model's ability to accurately pickup micro-seismic P- and S-waves in the presence of multiple arrival times of P- and S-waves.

To evaluate the performance of the LAU-Net model concerning processing speed and model complexity, we juxtapose it against the STA/LTA method, CAGNET+CNNDET, and U-Net++. Picking time and model size serve as the benchmarks for our assessment. The LAU-Net model showcases an 11.59ms reduction in inference time compared to the STA/LTA method. Moreover, it achieves a remarkable 8.5-fold improvement in inference speed in comparison to the CDDNET+CAGNET method. Additionally, the LAU-Net model exhibits a sixfold increase in inference speed when compared with the UNet++ method. This acceleration aligns with the Occam's razor principle, asserting that opting for a simpler model to attain comparable performance can mitigate the risk of overfitting. Regarding model size, the LAU-Net

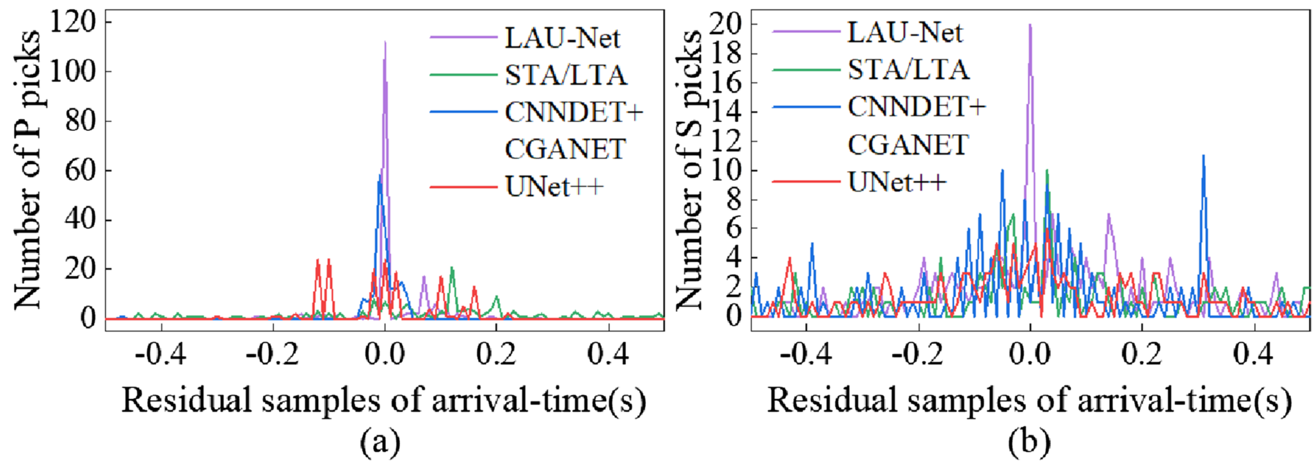

Fig. 7 **a** Error distribution of P-wave arrival-time **b** error distribution of S-wave arrival-time

model boasts a significantly smaller footprint, approximately one-sixth of the CDDNET+CAGNET method, and slightly surpasses the UNet++ model by around 1MB in parameters. This reduction in model size can be attributed to the LAU-Net model's substitution of regular convolution with Ghost convolution, resulting in fewer model parameters and enhanced inference speed. In summary, the LAU-Net model excels in striking a balance between precision and speed. Experimental results underscore its effectiveness and competitive performance. Furthermore, the application-aware loss function does not introduce an additional computational burden during the inference phase.

To visualize the precision of arrival time predictions by the LAU-Net model, histograms of P-wave and S-wave arrival-times errors from each method are presented in Fig. 7. Figure 7a illustrates the distribution of P-wave arrival-time errors, while Fig. 7b showcases the S-wave arrival-time errors. The experimental findings reveal that the LAU-Net model produces P-wave and S-wave time errors that exhibit a zero-centered error distribution. The majority of errors fall below 0.1s, aligning with a Gaussian distribution. Notably, the LAU-Net model outperforms the other three methods in terms of error distribution. This is because the STA/LTA method has difficulty in distinguishing and accurately determining the P- and S-wave arrivals in the case of containing both P- and S-waves, which makes the arrivals picked up by the STA/LTA method have a large error compared to the labeled results. The performance of the GRU unit and the self-attention mechanism module used in the CNNDET+CGANET method is affected by the length of the input sequence. The UNet ++ method's deep structure and multi-scale connectivity lead to higher computational complexity, especially when working with long sequences or large datasets. On the contrary, the applied perceptual loss function of the LAU-Net model improves the accuracy of the arrival pickup by combating different types of noise and learning complex micro-seismic P- and S-wave features.

Figure 8 depicts the pickup results for two micro-seismic signals. The black and red solid lines indicate the P-wave and S-wave time-of-arrival pickup results of the different methods for the signals in Fig. 8 (i), while the green and orange dashed lines correspond to the expert manual pickup results, respectively. From Fig. 8a, it can be seen that the errors of P-wave and S-wave arrival moments are 0 s and 0.8s for the STA/LTA method, 0.01s and 0.6s for the CNNDET+CAGNET method, 0 s and 0.1s for the UNet++ method, 0 s and 0.1s for the LAU-Net method, and 0 s and 0.1s for the UNet+ method, respectively. From Fig. 8b, it can be seen that the STA/LTA method picks up the P-wave and S-wave with an error of 0.1s and 0.76s, respectively; the CNNDET+CAGNET method picks up the P-wave and S-wave with an error of 0.02s and 0.86s, respectively; the UNet++ method picks up the P-wave and S-wave with an error of 0.1s and 0.6s, respectively; the UNet++ method picks up the P-wave and S-wave with an error of 0.1s and 0.1s, respectively; and the LAU-Net method picks up the P-wave and S-wave with an error of 0.1s and 0.1s, respectively, and S-wave to time error is 0.02s and 0.98s, respectively, and the LAU-Net method picks up P-wave and S-wave to time error is 0.01s and 0 s, respectively.

From the experimental findings, it becomes apparent that there are discernible inaccuracies in the P- and S-waves arrival-time determinations made by the STA/LTA, CNNDET+CGANET, and UNet++ methods, encompassing both incorrect and missed determinations. In contrast, the LAU-Net model produces results without any erroneous determinations or omissions. These disparities can be ascribed to various factors. The limitations of the STA/LTA method arise from the selection

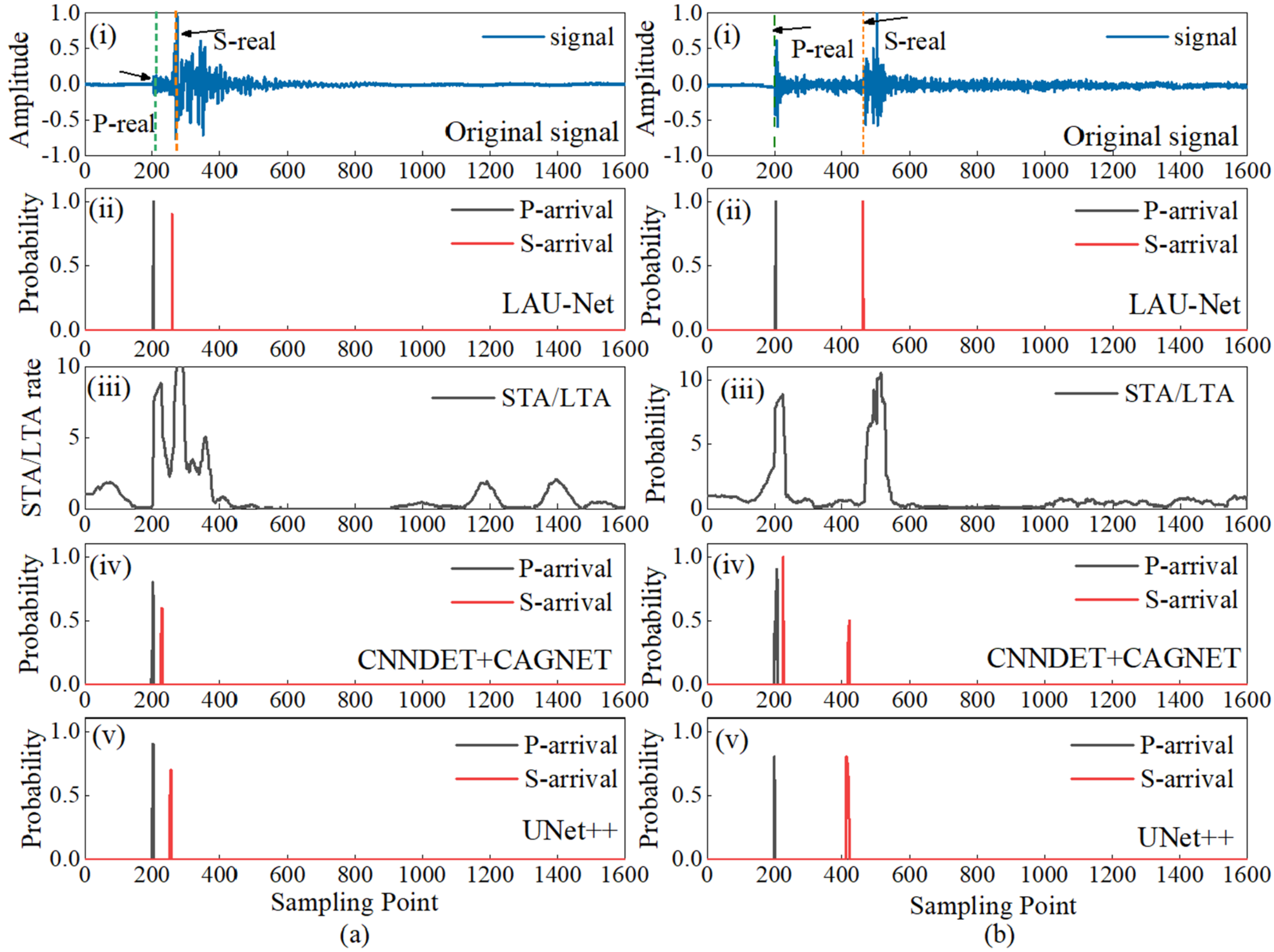

Fig. 8 Comparison of different methods for micro-seismic data pickup results with real results. **a** and **b** are two examples of micro-seismic P- and S-wave arrival-times pickup. (i) represents the micro-seismic waveform, (ii) is the probabilistic prediction curve of the P- and S-wave arrival-times positions for LAU-Net model, (iii) is the prediction curve of STA/LTA method, (iv) is the probabilistic prediction curve of the P- and S-wave arrival-times positions for CNNDET+CGANET method, and (v) is the probabilistic prediction curve of the P- and S-wave arrival-times positions for UNet++ method

of feature functions, which, when inadequately chosen, can result in erroneous determinations and omissions. The CNNDET+CGANET method, relying on two networks, introduces additional model parameters, leading to a slower determination process. Meanwhile, the UNet++ method, despite employing a residual connection that integrates micro-seismic waveform features, lacks a hybrid residual attention mechanism, resulting in redundant information extraction that interferes with P- and S-wave arrival-time determination. In contrast, the LAU-Net model excels at capturing correlation features between P- and S-waves with fewer parameters, thereby enhancing the arrival-time determination speed. Moreover, the designed GHRA layer effectively mitigates overfitting on smaller test sets. The application-aware loss function plays a crucial role in constraining the update direction of the determination network, facilitating a more comprehensive extraction of micro-seismic waveform sample features from the dataset without an excess of computational parameters. This ultimately leads to a more profound understanding of the dataset sample distribution and a notable improvement in P- and S-wave arrival-time determination precision. In summary, the LAU-Net model significantly enhances the precision of P- and S-wave arrival-time determinations, bringing them closer to actual results.

Application of pickup P- and S-waves in Sichuan oil field

To verify the seismic phase recognition effect of the LAU-Net model in different periods and its generalization ability, the paper uses the 2019–2020 micro-seismic dataset from Sichuan to test the LAU-Net model. The dataset is identified

Table 6 P- and S-wave pickup effects of the four different methods in the 2019–2020 Sichuan test set

Model	P-wave				S-wave				Params (M)	Time (ms)
	P	R	F1	MAE (s)	P	R	F1	MAE (s)		
LAU-Net	0.935	0.892	0.913	0.099s	0.914	0.882	0.898	0.164s	0.48	1.11
STA/LTA	0.728	0.735	0.731	0.204s	0.701	0.689	0.695	0.217s	\	12.7
CNNDET+CGANET	0.899	0.888	0.893	0.130s	0.768	0.729	0.748	0.191s	2.88	16.3
UNet++	0.876	0.861	0.868	0.278s	0.792	0.788	0.790	0.23s	1.50	8.9

using the LAU-Net model, and the results of P- and S-wave arrival time pickup are shown in Table 6.

The pickup accuracies of the 2019–2020 Sichuan oilfield micro-seismic dataset are shown in Table 6. As can be seen from Table 6, compared with the STA/LTA method, the LAU-Net model increases the P-wave and S-wave precision by 0.207, 0.213, the recall rate by 0.157, 0.193, and the F1 scores by 0.182, 0.203, and the average absolute error decreases by 0.105s, 0.053s. Compared with the CNNDET+CGANET method, the P-wave and S-wave pickup precision rises by 0.036, 0.146, the recall rate rises by 0.004, 0.153, the F1 score rises by 0.02, 0.15, and the mean absolute error drops by 0.031s, 0.027s. Compared with the UNet++ method, the P- wave and S-wave precision increased by 0.059 and 0.122, recall increased by 0.031 and 0.094, F1 score increased by 0.045 and 0.108, and average absolute error decreased by 0.179s and 0.066s, respectively. The experimental results show that compared with the STA/LTA, CNNDET+CGANET, and UNet++ methods, the LAU-Net model accuracy and speed are still the best, which is mainly because the pickup accuracy of STA/LTA is limited by the threshold setting, the source of timing information acquisition of UNet++ relies only on the convolutional layer, and the convolutional layer itself is weak for long sequence timing information grasping ability, so the pickup effect decreases inferiorly to the CNNDET+CGANET method and LAU-Net method. The autoregressive operation of the gated loop unit in the CNNDET+CGANET method cannot process the sequence information in parallel, which makes the model run inefficiently and slows down the recognition speed. However, the GHRA layer in the LAU-Net method can reduce the computational burden, correlate the features of micro-seismic P-wave and S-wave, be adaptable, and pickup high accuracy and speed. Meanwhile, the application-aware loss function designed in the thesis has a certain learning ability for the complex features of micro-seismic signals, which further improves the pickup P-wave and S-wave accuracy of the LAU-Net model. In addition, the designed application-aware loss function can be pre-trained in an offline environment, and real-time applications, LAU-Net only needs inference rather than training, which can accelerate the recognition process.

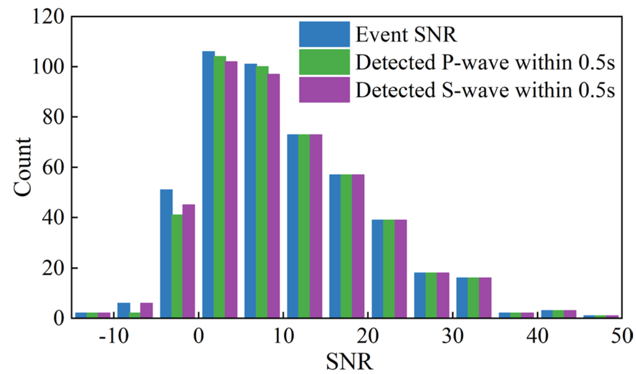

Fig. 9 Micro-seismic P-wave and S-wave picking results with different SNRs

Noise immunity tests

In the pragmatic context of shale gas resource extraction, noise becomes an unavoidable factor. To offer a more nuanced evaluation of the model's resilience to noise, the LAU-Net model underwent testing using micro-seismic waveforms at diverse SNR levels. The corresponding test outcomes are depicted in Fig. 9. In this visualization, the blue bar denotes the number of detected micro-seismic events, while the green and purple bars signify the P- and S-waves identified by LAU-Net. Notably, these results maintained errors below 0.5s. As illustrated in Fig. 9, the experimental findings suggest that the LAU-Net model excels in identifying P- and S-waves, particularly in conditions with higher SNR. Impressively, it consistently and accurately identifies a significant portion of P- and S-wave arrival times even in environments with lower SNR levels.

To thoroughly assess the proficiency of the LAU-Net model in accurately identifying micro-seismic P- and S-wave arrival times across diverse SNRs, Fig. 10 presents a comparative analysis between the results obtained by the LAU-Net model and the ground truth. In this representation, the green and orange dashed lines delineate the actual P- and S-wave arrival times, while the black and red solid lines portray the corresponding results detected by the LAU-Net model. Figure 10a–d illustrates six instances of

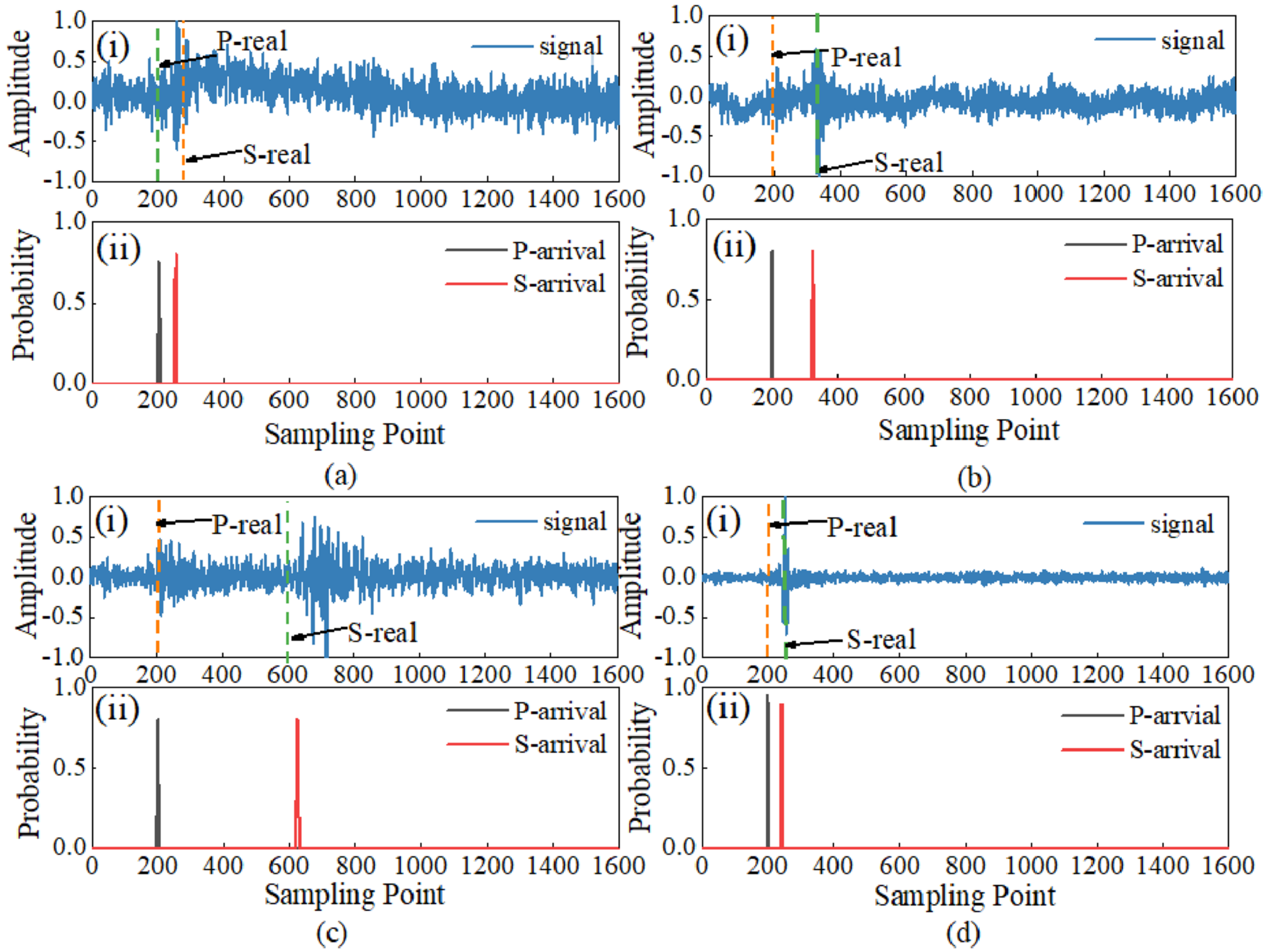

Fig. 10 Comparison of LAU-Net model pickup results with real results under different SNRs. For each subfigure, (i) is the micro-seismic waveform, and (ii) is the P- and S-wave arrival-times position probability prediction curves of the LAU-Net model; the SNRs of these micro-seismic events are **a** −5.155 dB, **b** 1.618 dB, **c** 3.472 dB, **d** 5.813 dB

micro-seismic waveforms with SNRs of −5.155 dB, 1.618 dB, 3.472 dB, and 5.813 dB, respectively. For these four instances, the absolute errors between the actual P-wave arrival times and those identified by the LAU-Net model are 0.05, 0.02, 0.02, and 0.04, respectively. Similarly, the absolute errors between the genuine S-wave arrival times and the corresponding results identified by the LAU-Net model are 0.11, 0.05, 0.04, and 0.29s. These experimental findings highlight the LAU-Net model's exceptional capability to mitigate noise interference. Its arrival-time confidence curves closely align with the actual labels, even in extreme cases where the SNR of the micro-seismic waveform is as low as -5.155dB. The GHRA layer within the LAU-Net model adeptly distinguishes various sources of noise in micro-seismic waveforms and assimilates the characteristics of micro-seismic P- and S-wave arrival times. In contrast to traditional methods that often misidentify noise as P/S-wave arrival times, the LAU-Net model excels in precisely identifying P- and S-wave arrival times, even in low SNR environments where noise can easily overshadow the target signals.

On-site, a plethora of noise types, encompassing impulse noise and periodic noise, are frequently encountered, leading to interference with micro-seismic waveforms. Impulse noise typically arises from mechanical or human-induced vibrations at the site, exhibiting amplitude and frequency characteristics akin to those of P- and S-waves at the point of arrival time. The primary distinction lies in their polarization characteristics, as elucidated in Fig. 11a. In contrast, periodic noise displays time-varying behavior and often shares frequency bands with micro-seismic waveforms, as illustrated in Fig. 11b. To comprehensively evaluate the resilience and effectiveness of the LAU-Net model in micro-seismic P- and S-wave arrival-time picking across diverse noise conditions, the experimental results manifest that the LAU-Net model excels in handling all types of

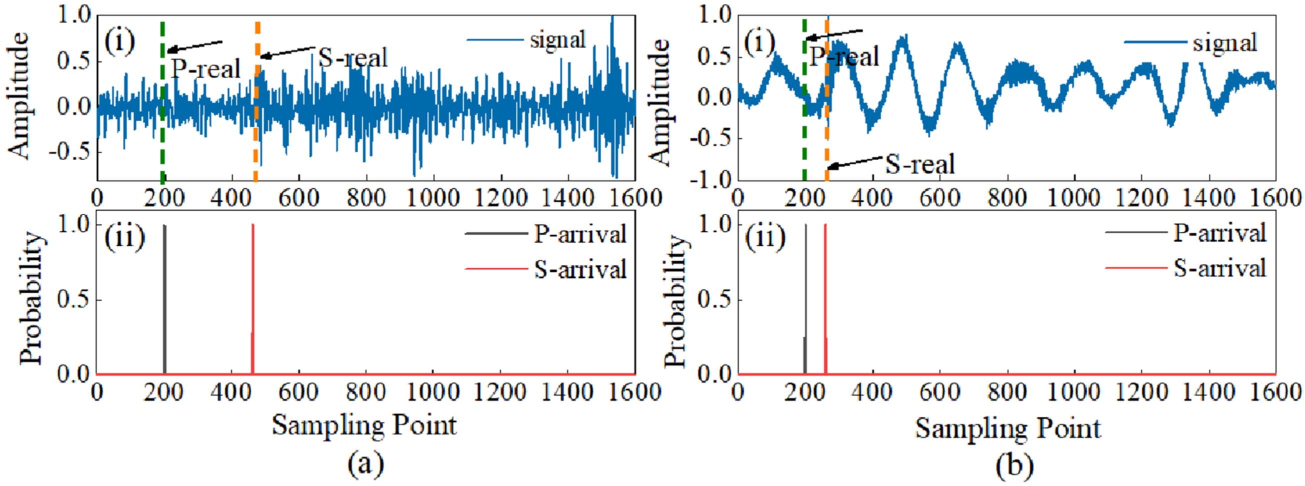

Fig. 11 Comparison of the LAU-Net model picking results with the real results under different types. **a** Comparison between micro-seismic model pickup and real results for micro-seismic waveforms under impulse noise **b** Comparison between micro-seismic model picking and real results for micro-seismic waveforms under periodic noise

noise data. It not only precisely determines arrival times but also adeptly mitigates interference. This exemplary performance can be attributed to the inclusion of an application-aware loss function in the LAU-Net model. This loss function places heightened emphasis on training with noisy samples, consistently constraining gradient updates in the pickup network, thereby enhancing precision in P- and S-wave arrival times. Furthermore, the LAU-Net model incorporates a hybrid attention mechanism within the GHRA layer. This mechanism learns to discriminate between the arrival time information of micro-seismic P- and S-waves and periodic noise, accurately focusing on the micro-seismic waveform arrival times. This feature ensures temporal consistency in the picked results with real labels, maintaining seismic precision, and ultimately enhancing pickup outcomes.

Drawback of LAU-net model

Examining the outcomes presented in Fig. 12, it becomes evident that while the LAU-Net model demonstrates strong performance on the test dataset encompassing 59 MS events within the − 15 to 0 dB SNR range, it successfully picked 45 P-waves and 53 S-waves. However, the precise detection rate of P-waves slightly lags behind that of S-waves. This occurrence stems from the relatively diminished amplitude of P-waves under low SNR conditions, rendering them susceptible to noise interference. Figure 12 also illustrates that S-waves exhibit more robust feature extraction and a heightened resilience to noise in comparison to P-waves, largely due to their lengthier waveform duration. In the two cases outlined in Fig. 12, (a) (i) displays some lingering noise preceding the P-wave's arrival time, leading to pick errors in the P-wave. Conversely, (b) (ii) directly experiences noise interference, causing the P-wave to be entirely overlooked. To address this challenge, a viable solution involves integrating noise reduction techniques into the MS waveform processing alongside P/S-wave arrival-times picking. By applying a simple mean filter before P/S-waves arrival-times determination, the adverse impact of noise on the P/S-waves arrival-times picking can be mitigated, as depicted in Fig. 12 (iii) and (iv).

On the other hand, in the realm of supervised models, the volume of data assumes paramount importance, and the presence of a substantial corpus of training data plays a pivotal role in enhancing model performance. Regrettably, the dataset available from the Sichuan Shengli oilfield's micro-seismic data, although it contains labeled instances, remains rather limited in scale. This inherent constraint poses challenges when aiming to satisfy the requirements of large-scale supervised deep learning. One viable remedy to this conundrum lies in the adoption of a semi-supervised learning paradigm. This entails utilizing unlabeled samples during model training, thereby diminishing the reliance on P- and S-wave labeled samples and ameliorating the potential sharp decline in picking performance occasioned by the paucity of labeled samples. As part of our future research endeavors, we intend to expand the existing dataset, amalgamating both labeled and unlabeled samples. This augmentation of data resources promises to render the P- and S-wave arrival times pickup model more adept and efficient. Nevertheless, this ambitious transition necessitates an adaptation of the current LAU-Net structure to align with the novel dataset's training requirements.

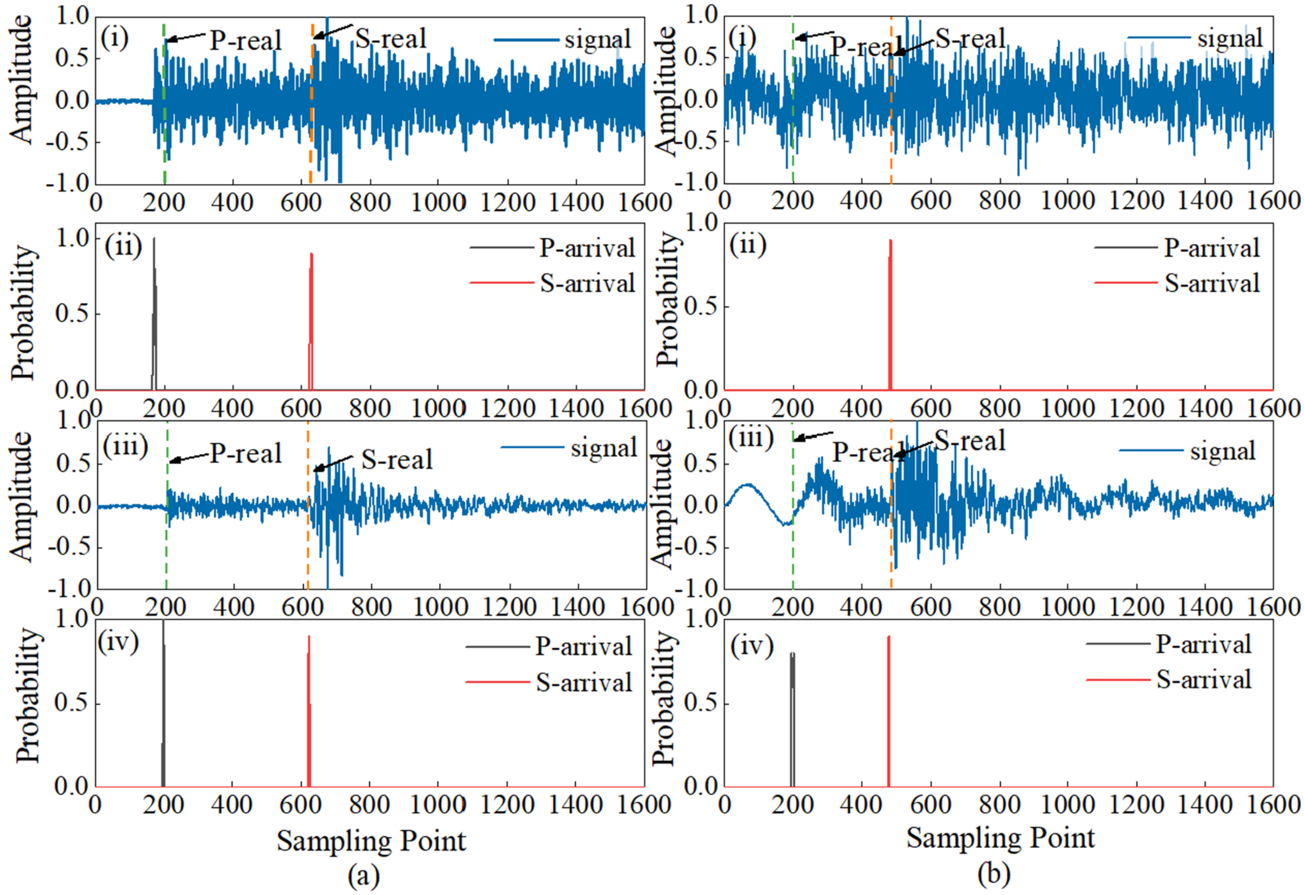

Fig. 12 Comparison of micro-seismic waveform picking results with real results by different methods. **a** and **b** are two examples of micro-seismic P- and S-wave pickup; (i) denotes the micro-seismic waveforms in the test set, (ii) shows the probability curves of P- and S-wave arrival times positions predicted by LAU-Net model for the micro-seismic waveforms in the test set, (iii) shows the micro-seismic waveforms after median filtering, and (iv) shows the probability curves of P- and S-wave arrival times positions picked up by LAU-Net model for the median filtered micro-seismic waveforms

Conclusions

In order to improve the microseismic P-wave and S-wave pickup accuracy and accelerate the pickup speed, the lightweight adversarial U-network (LAU-Net) is investigated in this paper. The pickup performance of the LAU-Net model is investigated through model design, simulation, and experiment. The results show that:

(1) The LAU-Net model has accurate and fast pickup capability for P- and S-waves in micro-seismic signals.
(2) The convolution kernel size selection experiment and layer optimization experiment show that the model performance is best in terms of accuracy and speed when the convolution kernel size is 5 and the number of GHRA layers is 4.
(3) The results of the ablation experiments show that both the GHRA layer and the application-aware loss function play a key role in the accurate and fast pickup of micro-seismic P- and S-wave arrival times by the LAU-Net model. Removing any GHRA layer and application-aware loss function will significantly reduce the pickup ability of the network.
(4) The results of anti-noise experiments show that the LAU-Net model can skillfully cope with various signal-to-noise ratios and different types of noisy data, and realize accurate P- and S-wave pickup.
(5) When applied to the actual project in the Shengli oilfield in Sichuan, the LAU-Net model performs well in effectively extracting micro-seismic P- and S-wave arrival times. Compared with the STA/LTA method, CNNDET+CGANet method, and UNet++ method, the LAU-Net model shows superior performance and practical application capability in terms of P- and S-wave arrival time pickup accuracy, model size, and pickup speed.

Author contributions JC wrote the manuscript and completely revised the paper. ZD wrote the manuscript. ZD and HC calculated and analyzed the signal data. FY provided suggestions for the research method. ZZ, RM and ZD summarized the findings. All authors have read and agreed to the published version of the manuscript.

Funding This research was funded by Science and Technology Innovation Program for Postgraduate students in IDP subsidized by Fundamental Research Funds for the Central Universities (Grant No. ZY20230324), the Self Fund Project of Langfang Science and Technology (Grant Nos. 2023011017) and the Key Laboratory Open Fund Project of Hebei Provincial (Grant Nos. FZ224105) and College Students' Innovation and Entrepreneurship Training Program Project of Institute of Disaster Prevention (Grant Nos. 202311775011).

Declarations

Conflict of interest The authors declare no Conflict of interest

References

Acar E, Türk O, Erturul F et al. (2021) Employing deep learning architectures for image-based automatic cataractdiagnosis. Turk J Electric Eng Comput Sci 29 (8):5. https://doi.org/10.3906/elk-2103-77

Alakbari FS, Mohyaldinn ME, Ayoub MA et al (2023) A gated recurrent unit model to predict Poisson's ratio using deep learning. J Rock Mech Geotech Eng 16 (2024):123–135. https://doi.org/10.1016/j.jrmge.2023.04.012

Alireza B, Mojdeh D (2023) Strategy for optimum chemical enhanced oil recovery field operation. J Resour Recov 1:1001. https://doi.org/10.52547/jrr.2208.1001

Allen RV (1978) Automatic earthquake recognition and timing from single traces. Bull Seismol Soc Am 68 (5):1521–1532. https://doi.org/10.1785/BSSA0680051521

Beyreuther RM, Barsch Krischer L, Megies T et al (2010) Automatic earthquake recognition and timing from single traces. Seismol Res Lett 81 (3):530–533. https://doi.org/10.1785/gssrl.81.3.530

Cai J, Dai X, Gao Z et al (2022) Automatic phase identification of earthquake based on the UBDN deep network. J Intell Fuzzy Syst 42 (6):5227–5236. https://doi.org/10.3233/JIFS-211792

Dandi A, Mohammed SAK, Moaz D et al (2023) Probabilistic estimation of hydraulic fracture half-lengths: validating the Gaussian pressure-transient method with the traditional rate transient analysis-method (wolfcamp case study). J Pet Explor Prod Technol 13:2475–2489. https://doi.org/10.1007/s13202-023-01680-9

Deyu Y, Yadong C, Yushun Y et al (2023) Research on interference signal recognition in p wave pickup and magnitude estimation. Geotech Geol Eng. https://doi.org/10.1007/s10706-023-02648-6

ERTURUL F (2019) A novel randomized recurrent artificial neural network approach: recurrent random vector functional link network. Turk J Electric Eng Comput Sci 27 (6):15. https://doi.org/10.3906/elk-1903-75

Fahd SA, Mysara EM, Mohammed AA et al (2021) Deep learning approach for robust prediction of reservoir bubble point pressure. ACS Omega 6 (33):21499–21513. https://doi.org/10.1021/acsomega.1c02376

Fahd SA, Mysara EM, Mohammed AA et al (2023) A robust Gaussian process regression-based model for the determination of static young's modulus for sandstone rocks. Neural Comput and Applic 35:15693–15707. https://doi.org/10.1007/s00521-023-08573-2

Goodfellow I, Pouget-Abadie J, Mirza M et al (2020) Generative adversarial networks. Commun ACM 63 (11):139–144. https://doi.org/10.1145/3422622

Guo C, Zhu T, Gao Y et al (2021) Aenet: automatic picking of p-wave first arrivals using deep learning. IEEE Trans Geosci Remote Sens 59:5293–5303. https://doi.org/10.1109/TGRS.2020.3010541

Guo X (2021) First-arrival picking for microseismic monitoring based on deep learning. Int J Geophys 2021:1–14. https://doi.org/10.1155/2021/5548346

Han K, Wang Y, Xu C et al (2022) Ghostnets on heterogeneous devices via cheap operations. Int J Comput Vis 130 (4):1050–1069. https://doi.org/10.1007/s11263-022-01575-y

Hou X, Zheng YJM et al (2023) Sea-net: sequence attention network for seismic event detection and phase arrival picking. Eng Appl Artific Intell Int J Intell Real-Time Autom 122:106090. https://doi.org/10.1016/j.engappai.2023.106090

Jiao M, Fangjie D, Hao L et al (2023) A method for picking up the arrival time of mining microseismic p-waves by integrating gated cyclic units and self attention mechanisms. J Seismol 45 (02):234–245. https://doi.org/10.11939/jass.20220034

Jolicoeur-Martineau A (2018) The relativistic discriminator: a key element missing from standard GAN. CoRR abs/1807.00734. https://doi.org/10.48550/arXiv.1807.00734

Kingma DP, Ba J (2014) Adam: a method for stochastic optimization. arXiv preprint arXiv:1412.6980https://doi.org/10.48550/arXiv.1412.6980

Lan Z, Gao P, Wang P et al (2022) Automatic first arrival time identification using fuzzy c-means and AIC. IEEE Trans Geosci Remote Sens 60:1–13. https://doi.org/10.1109/TGRS.2021.3121032

Li Y, Xu C, Han J et al (2022) Mhau-net: skin lesion segmentation based on multi-scale hybrid residual attention network. Sensors 22:8701. https://doi.org/10.3390/s22228701

Long Y, Lin J, Huang X et al (2023) Automatic microseismic event detection with variance fractal dimension via multitrace envelope energy stacking. IEEE Trans Geosci Remote Sens 60:1–15. https://doi.org/10.1109/TGRS.2021.3138899

Mao X, Li Q, Xie H et al (2017) Least squares generative adversarial networks. Proc IEEE Int Conf Comput Vis 60:2794–2802. https://doi.org/10.48550/arXiv.1611.04076

Ni F, He Z, Jiang S et al (2022) A generative adversarial learning strategy for enhanced lightweight crack delineation networks. Adv Eng Inf. https://doi.org/10.1016/j.aei.2022.101575

Tang S, Wang J, Tang C (2021) Identification of microseismic events in rock engineering by a convolutional neural network combined with an attention mechanism. Rock Mech Rock Eng 54:47–69. https://doi.org/10.1007/s00603-020-02259-0

Tiwari RK, Rajesh R (2021) Advances in geo-time series modelling. J Geol Soc India 97:1313–1322. https://doi.org/10.1007/s12594-021-1862-4

Xu H, Zhao Y, Yang T et al (2022) An automatic p-wave onset time picking method for mining-induced microseismic data based on long short-term memory deep neural network. Nat Hazards Risk 13 (1):908–933. https://doi.org/10.1080/19475705.2022.2057241

Xu J, Yang L, Liu Z et al (2021) A new approach to embed complex fracture network in tight oil reservoir and well productivity analysis. Nat Resour Res 30:2575–2586. https://doi.org/10.1007/s11053-021-09845-1

Xu L, Chen Y (2021) Easy detection for the high-pass filter cut-off frequency of digital ground motion record based on STA/LTA method: a case study in the 2008 Wenchuan mainshock. J Seismol 25:1281–1300. https://doi.org/10.1007/s10950-021-10034-z

Yao Y, Liu L (2022) Automatic p-wave arrival picking based on inaction method. IEEE Trans Geosci Remote Sens 60:1–11. https://doi.org/10.1109/TGRS.2022.3230411